arXiv:astro-ph/0408420v1 23 Aug 2004

Anomalously low PAH emission from low-luminosity galaxies

David W. Hogg[1,2], Christy A. Tremonti[3], Michael R. Blanton[1], Douglas P. Finkbeiner[4], Nikhil Padmanabhan[5], Alejandro D. Quintero[1], David J. Schlegel[4], and Nicholas Wherry[1]

ABSTRACT

The Spitzer Space Telescope First Look Survey Infrared Array Camera (IRAC) near and mid-infrared imaging data partially overlaps the Sloan Digital Sky Survey (SDSS), with 313 visually selected ($r < 17.6$ mag) SDSS Main Sample galaxies in the overlap region. The 3.5 and 7.8 μm properties of the galaxies are investigated in the context of their visual properties, where the IRAC [3.5] magnitude primarily measures starlight, and the [7.8] magnitude primarily measures PAH emission from the interstellar medium. As expected, we find a strong inverse correlation between $[3.5] - [7.8]$ and visual color; galaxies red in visual colors ("red galaxies") tend to show very little dust and molecular emission (low "PAH-to-star" ratios), and galaxies blue in visual colors ("blue galaxies," *i.e.*, star-forming galaxies) tend to show large PAH-to-star ratios. Red galaxies with high PAH-to-star ratios tend to be edge-on disks reddened by dust lanes. Simple, visually inferred attenuation corrections bring the visual colors of these galaxies in line with those of face-on disks; *i.e.*, PAH emission is closely related to attenuation-corrected, optically inferred star-formation rates. Blue galaxies with anomalously low PAH-to-star ratios are all low-luminosity star-forming galaxies. There is some weak evidence in this sample that the deficiency in PAH emission for these low-luminosity galaxies may be related to emission-line metallicity.

Subject headings: dust, extinction — galaxies: dwarf — galaxies: evolution — galaxies: general — galaxies: ISM — infrared: galaxies — ISM: general — surveys

1. Introduction

The Spitzer Space Telescope (Werner *et al.* 2004) is opening a new window in the Universe, with unprecedented sensitivity, angular resolution, and spectral coverage in the mid-infrared and

[1] Center for Cosmology and Particle Physics, Department of Physics, New York University, 4 Washington Pl, New York, NY 10003

[2] david.hogg@nyu.edu

[3] Steward Observatory, 933 N Cherry Ave, Tucson, AZ 85721

[4] Princeton University Observatory, Princeton, NJ 08544

[5] Department of Physics, Princeton University, Princeton, NJ 08544

far-infrared. The Spitzer Team has made Spitzer's first science data, its "First Look Survey" (FLS), immediately public. The extragalactic component of the FLS is in a field studied photometrically and spectroscopically in the visual as part of the Sloan Digital Sky Survey (SDSS; York *et al.* 2000; Abazajian *et al.* 2004). This overlap permits study of a large sample of normal, visually selected galaxies, with known redshifts and visual spectra, in the Spitzer bands.

One of the very exciting capabilities of Spitzer is mid-infrared imaging with the Infrared Array Camera (IRAC; Fazio *et al.* 2004). The longest-wavelength channel (centered at wavelength $\lambda = 7.8$ μm) is most sensitive to large, positive spectral features coming from PAHs associated with interstellar dust (*e.g.*, Li & Draine 2001; Lu *et al.* 2003; Smith *et al.* 2004). Since dust is closely associated with star-formation, mid-infrared emission is strongly related to galaxy star formation (*e.g.*, Roche *et al.* 1991; Roussel *et al.* 2001; Lu *et al.* 2003; Förster Schreiber *et al.* 2004; Pahre *et al.* 2004; Willner *et al.* 2004) and promises to reveal a lot about galaxy formation and evolution. Unfortunately, no large, complete samples of galaxies have been studied to date.

The interstellar medium not only traces star formation but also obscures it. PAH emission is an indirect and nonlinear tracer of star formation activity, but at the same time it is expected to be an order of magnitude less attenuated by dust than the direct measures of young stellar populations in the visible (emission lines) and ultraviolet (thermal continuum). For this reason, Spitzer observations have the potential to measure star-formation rates more fairly and to test dust corrections, which depend not just on dust abundance but also dust grain properties and dust geometry (*e.g.*, Calzetti 2001, and references therein).

One star-forming galaxy with apparently anomalous (termed "extraordinary") mid-infrared properties is the $M_B = -17.2$ mag dwarf galaxy SBS0335−052, which has metallicity $12 + \log_{10}(\mathrm{O/H}) = 7.338$ (Izotov *et al.* 1999), about 1/20 Solar (Allende Prieto, Lambert, & Asplund 2001). This dwarf shows a deficiency of PAH emission (Houck *et al.* 2004) despite strong star formation activity. Whether or not this galaxy is extraordinary, it certainly demonstrates that galaxies will show diverse properties in the Spitzer bandpasses.

Here we look at Spitzer IRAC fluxes from normal galaxies from the SDSS spectroscopic sample, to begin an investigation of the diversity of mid-infrared properties and their relationships with visual properties.

2. SDSS data

The SDSS data used here are well described in the SDSS Data Release 2 literature (Abazajian *et al.* 2004, and references therein). The visual photometric measurements on the data used here are discussed in detail elsewhere (Blanton *et al.* 2003b) and only briefly described here.

The SDSS g, r, and i Petrosian (Petrosian 1976) magnitudes are corrected for Galactic extinction with the SFD maps (Schlegel *et al.* 1998) and K corrected with the `kcorrect v3_2` package

(Blanton *et al.* 2003a), *not* to redshift $z = 0$ but to roughly the median redshift of $z = 0.1$. The rest-frame bandpasses thus made are effectively "blueshifted" by a factor of 1.1 and called ${}^{0.1}g$, ${}^{0.1}r$, and ${}^{0.1}i$. Calibration is to the AB system (Oke & Gunn 1983). Absolute magnitudes are computed in the ${}^{0.1}i$ band in the standard way (Hogg 1999), assuming a cosmological world model with $H_0 = 70\,h$ km s^{-1} Mpc^{-1}, $\Omega_M = 0.3$, and $\Omega_\Lambda = 0.7$.

The SDSS software fits various models to each galaxy image, below we use the axis ratio b/a for the best-fit ellipsoidal exponential model in the observed i band.

In each SDSS spectrum, Hα, Hβ, [O III] 5007 Å(hereafter just "[O III]"), and [N II] 6584 Å(hereafter just "[N II]") line fluxes are measured in 20 Å width intervals centered on each line. Before the flux is computed, the best-fit two-component SED model spectrum (from Quintero *et al.* 2004) is scaled to have the same flux continuum as the data in the vicinity of the emission line and subtracted to leave a continuum-subtracted line spectrum. This method fairly accurately models the Hα absorption trough in the continuum, although in detail it underestimates the Hα fluxes by, typically, a few percent (Quintero *et al.* 2004).

To each galaxy's spectrum (taken through a well-centered circular fiber with a 3 arcsec diameter), a model of star formation history and dust attenuation is fit, providing a visual estimate of the internal attenuation of starlight due to that galaxy's interstellar medium. We have designed a special-purpose code which fits a stellar population model to the galaxy continuum and estimates the attenuation of the starlight, under the assumption that any galaxy star formation history can be approximated as a sum of discrete bursts. The library of template spectra is composed of single stellar population models generated by population synthesis (Bruzual & Charlot 2003). The models incorporate an empirical spectral library (Le Borgne et al. 2003) with a wavelength coverage (3200 - 9300 Å) and spectral resolution (~ 3 Å) which is well matched to that of the SDSS spectral data. The templates include models of ten different ages (0.005, 0.025, 0.1, 0.2, 0.6, 0.9, 1.4, 2.5, 5, 10 Gyr) and three metallicities (1/5 $Z_\odot$, $Z_\odot$, and 2.5 $Z_\odot$). For each galaxy the templates are transformed to the appropriate redshift and velocity dispersion and resampled to match the data. A non-negative least squares is performed with dust attenuation modeled as an additional free parameter. The attenuation model is that the observed flux F_{obs} is related to the intrinsic flux F_i by $F_{obs} = F_i e^{-\tau_\lambda}$, where $\tau_\lambda \propto \lambda^{-0.7}$ (Charlot & Fall 2000). The fit of the models to the data is performed from 3600 to 8500 Å in the galaxy rest frame with the emission lines masked out. In practice, our ability to simultaneously recover age, metallicity, and attenuation is strongly limited by the signal-to-noise of the data. Hence we model galaxies as single metallicity populations and select the metallicity which yields the minimum χ^2. (While this is not particularly physical, in practice it is not a bad assumption since the integrated light of a galaxy tends to be dominated by the light of its most recent stellar generation.)

3. Spitzer data

The FLS data, like most IRAC data, were taken as a set of hundreds of pointings with the 256×256 IRAC arrays (with 1.2×1.2 arcsec^2 pixels). Each of these pointings gets passed through the Spitzer "basic calibrated data" (BCD) pipeline in which it is flatfielded and calibrated and in which cosmic rays and other bad pixels are identified and flagged.

For each galaxy in the SDSS sample, we identified all individual IRAC BCD images in which it appears and performed, in each one, aperture photometry through 9.2 arcsec diameter apertures. Background (or sky level) for each aperture flux was determined by taking a median in an annulus of inner radius 18 arcsec and outer radius 28 arcsec. Images with bad pixels or cosmic rays inside the inner aperture (according to the Spitzer-provided mask files) were excised and the photometry of the remaining images in each band for each galaxy was averaged together (possible because there are multiple "dithers" per pointing). The measurements were converted to AB magnitudes (Oke & Gunn 1983). We applied no K corrections to the Spitzer photometry.

4. Results

Figure 1 shows the observed Spitzer IRAC [3.5] − [7.8] color as a function of rest-frame visual color, with symbol size (major axis) linearly related to the logarithm of luminosity and shape showing the axis ratio of the image in the i band. Figure 2 shows the Spitzer color as a function of rest-frame visual absolute magnitude (luminosity). In Figure 1 a clear, strong relationship between visual color and infrared color is seen, with visually red galaxies showing blue infrared colors and visually blue galaxies showing red infrared colors. This trend has a natural explanation: blue galaxies are forming stars, star-forming galaxies contain dust, and dust produces PAH emission features in the [7.8] band. Red galaxies are old and dead; they have no material from which to make stars, therefore no dust or PAH features.

Visually red galaxies with red infrared colors tend to be dusty, edge-on galaxies, with high inferred visual attenuations. Figure 3 shows the same data as Figure 1 but de-reddened assuming the best-fit attenuation amplitude (described above) and the trivial $\lambda^{-0.7}$ attenuation law. This procedure is crude and not expected to be correct in detail for any of the sample galaxies.

It is remarkable that the crude and uniform galaxy-by-galaxy attenuation correction does a very good job of placing the visually red but infrared blue galaxies back into the main trend in Figure 1. This is a strong endorsement of the attenuations inferred from the SDSS spectrum analysis and suggests that simple attenuation corrections work well for normal galaxies.

The only remaining outliers on Figures 1 and 3 are visually blue galaxies with bluer-than-typical infrared colors for their visual color. The symbol sizes on the Figures show that these galaxies are low-luminosity galaxies. Evidently low-luminosity galaxies tend to be deficient in PAH-producing (and visually extinguishing) dust. This fits very well with the results on SBS0335−052, which

show a dwarf galaxy deficient in mid-infrared PAH emission. Indeed, it has been found in visual observations that there is a strong relationship between a disk galaxy's mass and its apparent interstellar medium content or state (Dalcanton *et al.* 2004).

If this effect—anomalous interstellar medium content in low-luminosity galaxies—is due to metallicity, a trend should show up in Figure 4, which shows infrared color as a function of line ratio [N II]/Hα for the dwarf galaxies for whom that ratio is measured to within a factor of three. This line ratio is a metallicity indicator with

$$12 + \log_{10}\left(\frac{\mathrm{O}}{\mathrm{H}}\right) \approx 9.12 + 0.73\ \log_{10}\left(\frac{[\mathrm{N\,II}]}{\mathrm{H}\alpha}\right) \quad (1)$$

(Denicoló, Terlevich, & Terlevich 2002; Kewley & Dopita 2002). While it is tempting to interpret the Figure as showing a dependency of PAH emission on metallicity, given the small sample and large errors, it shows no iron-clad trend in this sample. It is worth noting that none of the galaxies in this sample are likely to have metallicities nearly as low as that of SBS0335−052. Figure 5 is similar to Figure 4, but showing radiation field hardness indicator [O III]/Hβ. No trend is visible.

Figure 6 shows SDSS and IRAC images of some of the lower redshift galaxies in the sample, which are better resolved in the imaging, and include low luminosity members. It is clear that for the high luminosity galaxies, the [3.5] − [7.8] color is a very good predictor for attenuation-corrected visual color. This is consistent with the hypothesis that for these galaxies [7.8] flux traces star formation and [3.5] flux traces old stellar populations (Pahre *et al.* 2004). The outliers from this are all low in luminosity; the low luminosity galaxies tend to be deficient in [7.8] flux.

No K corrections have been applied to the IRAC data. Can the dependence on luminosity in fact be a failure to K correct (since the low luminosity galaxies are, on average, at lower redshifts)? There is a large, positive PAH feature in most galaxy spectra at around 7.7 μm (Li & Draine 2001; Lu *et al.* 2003; Smith *et al.* 2004) that will tend to make higher redshift galaxies (and therefore higher luminosity galaxies in this sample) *lower* in observed-frame [7.8] flux. Also, the low-redshift population in this sample actually spans a large luminosity range (see Figure 6), within which the luminosity trend of PAH emission is strong. For these reasons we conclude that the trends we see are not due to the failure to K correct.

5. Discussion

Luminous, star-forming galaxies are dusty, and old, red galaxies are dust-free.

This first look at the Spitzer First Look Survey does not show the IRAC photometry "diversifying" the luminous galaxy population beyond what is seen in the visual. In fact, the visual color, shape, luminosity, and spectrum of a luminous galaxy provides an extremely good prediction for its dust content and hence its Spitzer IRAC colors. PAH emission is a very good tracer of star formation for these luminous galaxies.

Low-luminosity galaxies show a deficiency in PAH emission. They also show much more diversity in PAH-to-star ratio; they will clearly provide a very important subject of study for Spitzer. Dwarfs could be PAH deficient because they tend to be low in metallicity (*i.e.*, lack the material to make PAHs), because they are low in mass (*i.e.*, lack the gravitational potential to retain dust and molecules against radiation pressure and winds), because they are young (*i.e.*, have lacked the time necessary to make PAHs), or because they have hard internal radiation fields (*i.e.*, have destroyed their PAHs). Low metallicity is the simplest explanation in many ways; indeed we have presented weak evidence for a dependence of the PAH-to-star ratio on metallicity among the low-luminosity galaxies. It is also possible that the dwarfs are not PAH deficient, but simply have different interstellar medium geometry or different relationships between molecules and radiation fields such that the molecules do not produce apparent emission in the [7.8] bandpass.

The strong, broad spectral features in the mid-IR from PAHs hold great promise for use in photometric redshift determinations (*e.g.*, Simpson & Eisenhardt 1999). The fact that PAH emission is a strong function of luminosity (or metallicity) may add complications to photometric redshift schemes—because not all galaxies are drawn from the same the same family of spectral energy distributions, and because there might be significant families of galaxies that lack the highly featured spectral energy distributions that are great for redshift inference. Of course any dependence of spectrum morphology on luminosity can also be very useful, since inference of luminosities is often the goal of photometric redshift determinations. Dependencies of spectral energy distributions on luminosity will also be important for accurate K corrections and bolometric corrections.

Because PAHs are (presumably) formed as stars evolve, the distribution, properties, and demographics of PAHs in galaxies of different types ought to contain information about galaxy formation and evolution; observations of these PAHs will be part of Spitzer's important legacy.

We thank the entire Spitzer Space Telescope project for starting the mission with a public legacy project. We thank Aaron Barth, Eric Bell, Julianne Dalcanton, Bruce Draine, Rob Kennicutt, Wayne Landsman, Mike Pahre, Bill Reach, and Lisa Storrie-Lombardi for useful data, discussions, information, or software.

The Spitzer Space Telescope is a mission of NASA. Funding for the creation and distribution of the SDSS has been provided by the Alfred P. Sloan Foundation, the Participating Institutions, NASA, the NSF, the U.S. Department of Energy, the Japanese Monbukagakusho, and the Max Planck Society. The Participating Institutions are The University of Chicago, Fermilab, the IAS, the Japan Participation Group, JHU, LANL, MPIA, MPA, NMSU, University of Pittsburgh, Princeton University, USNO, and the University of Washington. This research also made use of the NASA Astrophysics Data System. DWH, MRB, ADQ, and NW are partially supported by NASA (grant NAG5-11669) and NSF (grant PHY-0101738).

REFERENCES

Abazajian, K. *et al.* 2004, AJ, in press (Data Release Two)

Allende Prieto, C., Lambert, D. L., & Asplund, M. 2001, ApJ, 556, L63

Blanton, M. R., Brinkmann, J., Csabai, I., Doi, M., Eisenstein, D. J., Fukugita, M., Gunn, J. E., Hogg, D. W., & Schlegel, D. J. 2003a, AJ, 125, 2348

Blanton, M. R. *et al.* 2003b, ApJ, 594, 186

Bruzual, G. & Charlot, S., MNRAS, 344, 1000

Calzetti, D. 2001, PASP, 113, 1449

Charlot, S. & Fall, S. M. 2000, ApJ, 539, 718

Dalcanton, J. J., Yoachim, P., & Bernstein, R. A. 2004, ApJ, 608, 189

Denicoló, G., Terlevich, R., & Terlevich, E. 2002, MNRAS, 330, 69

Fazio, G. G. *et al.* 2004, ApJS, in press, (astro-ph/0405616)

Förster Schreiber, N. M., Roussel, H., Sauvage, M., & Charmandaris, V. 2004, A&A, 419, 501

Hogg, D. W. 1999, astro-ph/9905116

Houck, J. R. *et al.* 2004, ApJS, in press, (astro-ph/0406150)

Izotov, Y. I., Chaffee, F. H., Foltz, C. B., Green, R. F., Guseva, N. G., & Thuan, T. X. 1999, ApJ, 527, 757

Kewley, L. J. & Dopita, M. A. 2002, ApJS, 142, 35

Le Borgne, J. -F., Bruzual, G., Pelló, R., Lançon, A., Rocca-Volmerange, B., Sanahuja, B., Schaerer, D., Soubiran, C., Vílchez-Gómez, R. 2003, A&A, 402, 433

Li, A. & Draine, B. T. 2001, ApJ, 554, 778

Lu, N., Helou, G., Werner, M. W., Dinerstein, H. L., Dale, D. A., Silbermann, N. A., Malhotra, S., Beichman, C. A., & Jarrett, T. H. 2003, ApJ, 588, 199

Lupton, R., Blanton, M. R., Fekete, G., Hogg, D. W., O'Mullane, W., Szalay, A., & Wherry, N. 2004, PASP, 116, 133

Oke, J. B. & Gunn, J. E. 1983, ApJ, 266, 713

Pahre, M. A. *et al.* 2004, ApJS, in press, (astro-ph/0405594)

Petrosian, V. 1976, ApJ, 209, L1

Quintero, A. D. *et al.* 2004, ApJ, 602, 190

Roche, P. F., Aitken, D. K., Smith, C. H., & Ward, M. J. 1991, MNRAS, 248, 606

Roussel, H., Sauvage, M., Vigroux, L., & Bosma, A. 2001, A&A, 372, 427

Schlegel, D. J., Finkbeiner, D. P., & Davis, M. 1998, ApJ, 500, 525

Simpson, C. & Eisenhardt, P. 1999, PASP, 111, 691

Smith, J. D. T. *et al.* 2004, ApJS, in press (astro-ph/0406332)

Werner, M. W. *et al.* 2004, ApJS, in press (astro-ph/0406223)

Willner, S. P. *et al.* 2004, ApJS, in press, (astro-ph/0405626)

York, D. *et al.* 2000, AJ, 120, 1579

This preprint was prepared with the AAS LaTeX macros v5.2.

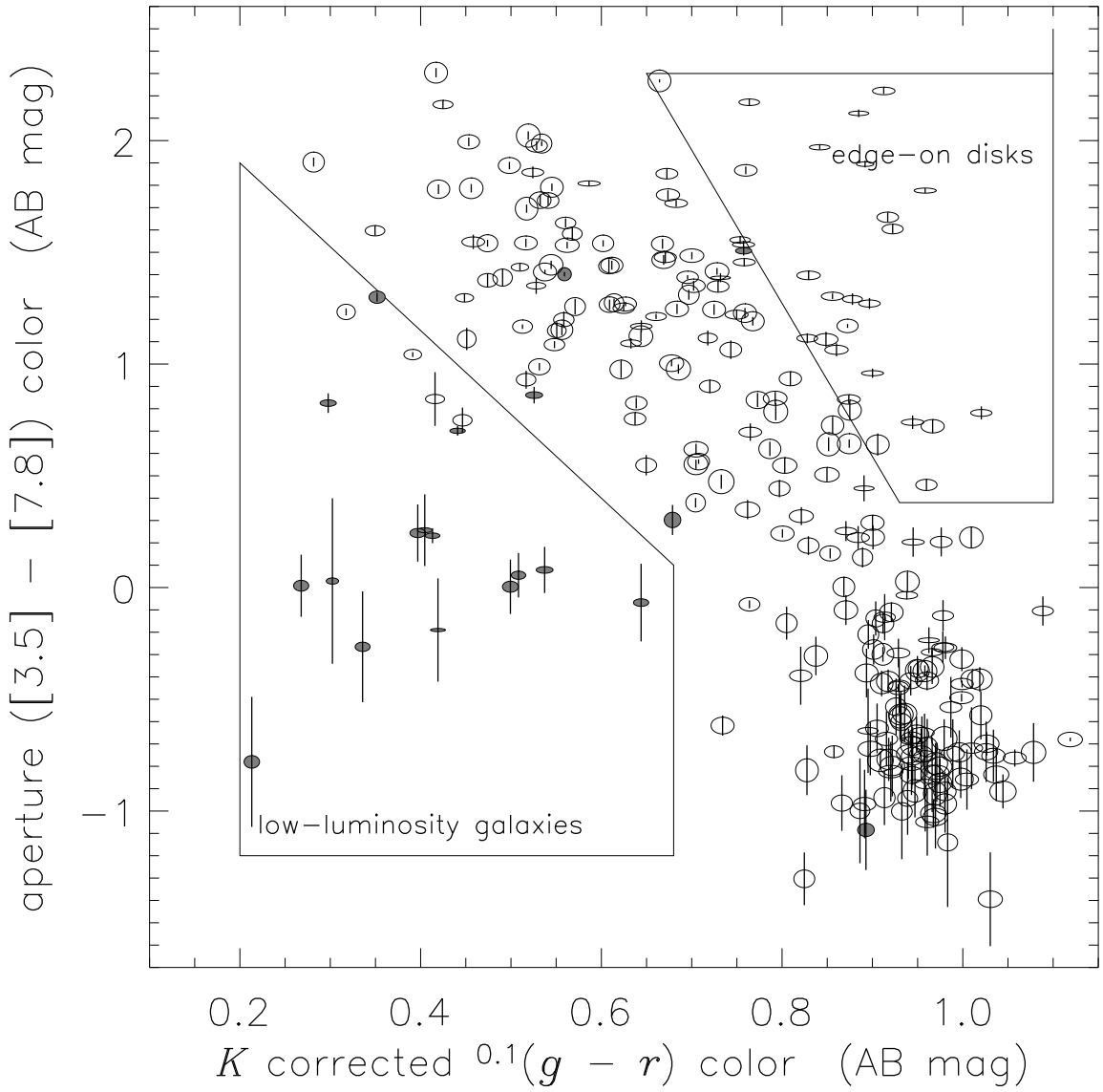


Fig. 1.— Spitzer IRAC observed-frame color (aperture fluxes explained in text) as a function of rest-frame visual color (blueshifted SDSS bandpasses explained in text). Symbol major axis (horizontal extent) is linearly related to log luminosity in the $^{0.1}i$ band (smaller symbols mean lower luminosities; compare to Figure 2), and the symbol shape shows the galaxy shape as observed on the sky. Galaxies with very low luminosities $M_{0.1i} > -19$ mag are filled with grey. Visually blue galaxies tend to have high dust-to-star ratios and therefore red $[3.5] - [7.8]$ colors; visually red galaxies tend to have low dust-to-star ratios and therefore blue $[3.5] - [7.8]$ colors. Exceptions are in the outlined regions: Red galaxies with high dust-to-star ratios tend to be edge-on disk galaxies reddened by their own dust. Blue galaxies with low dust-to-star ratios tend to be low-luminosity galaxies.

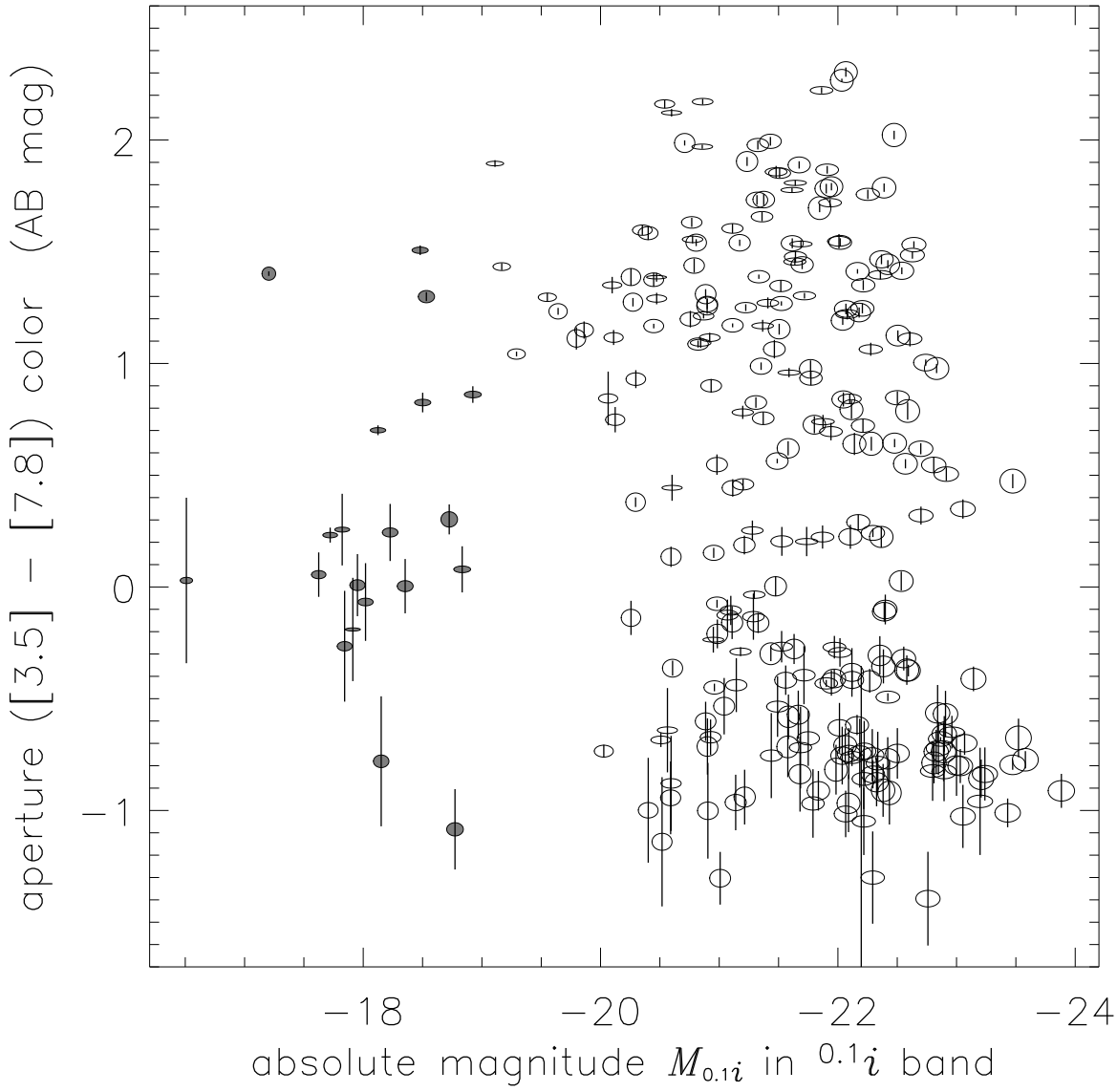


Fig. 2.— Spitzer IRAC observed-frame color as a function of rest-frame visual absolute magnitude (in the blueshifted SDSS i bandpass explained in text). Symbols as in Figure 1.

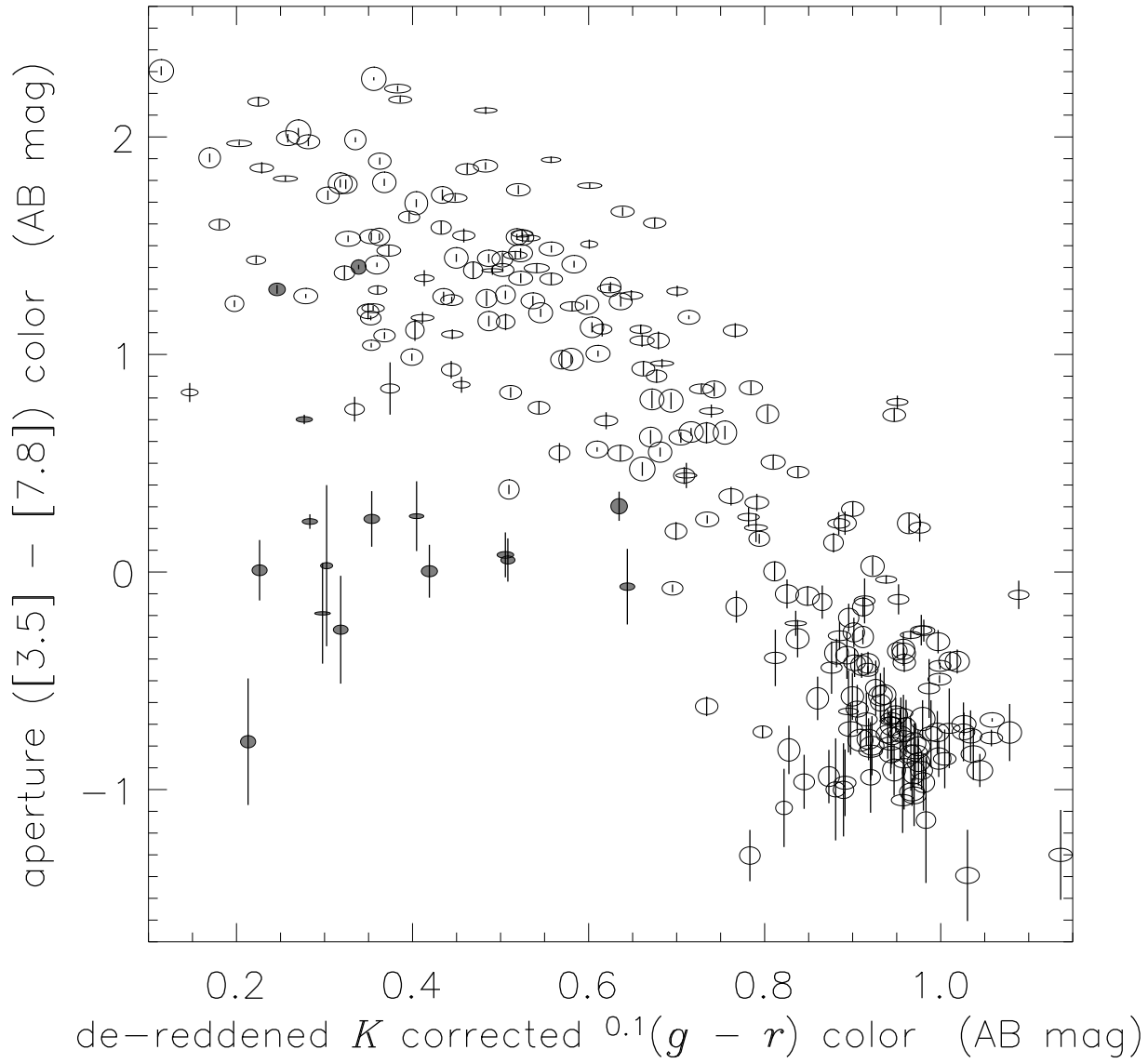


Fig. 3.— Same as Figure 1 but with reddening corrections applied (see text for details). The edge-on galaxies are no longer outliers from the main trend, but the low-luminosity galaxies remain outliers.

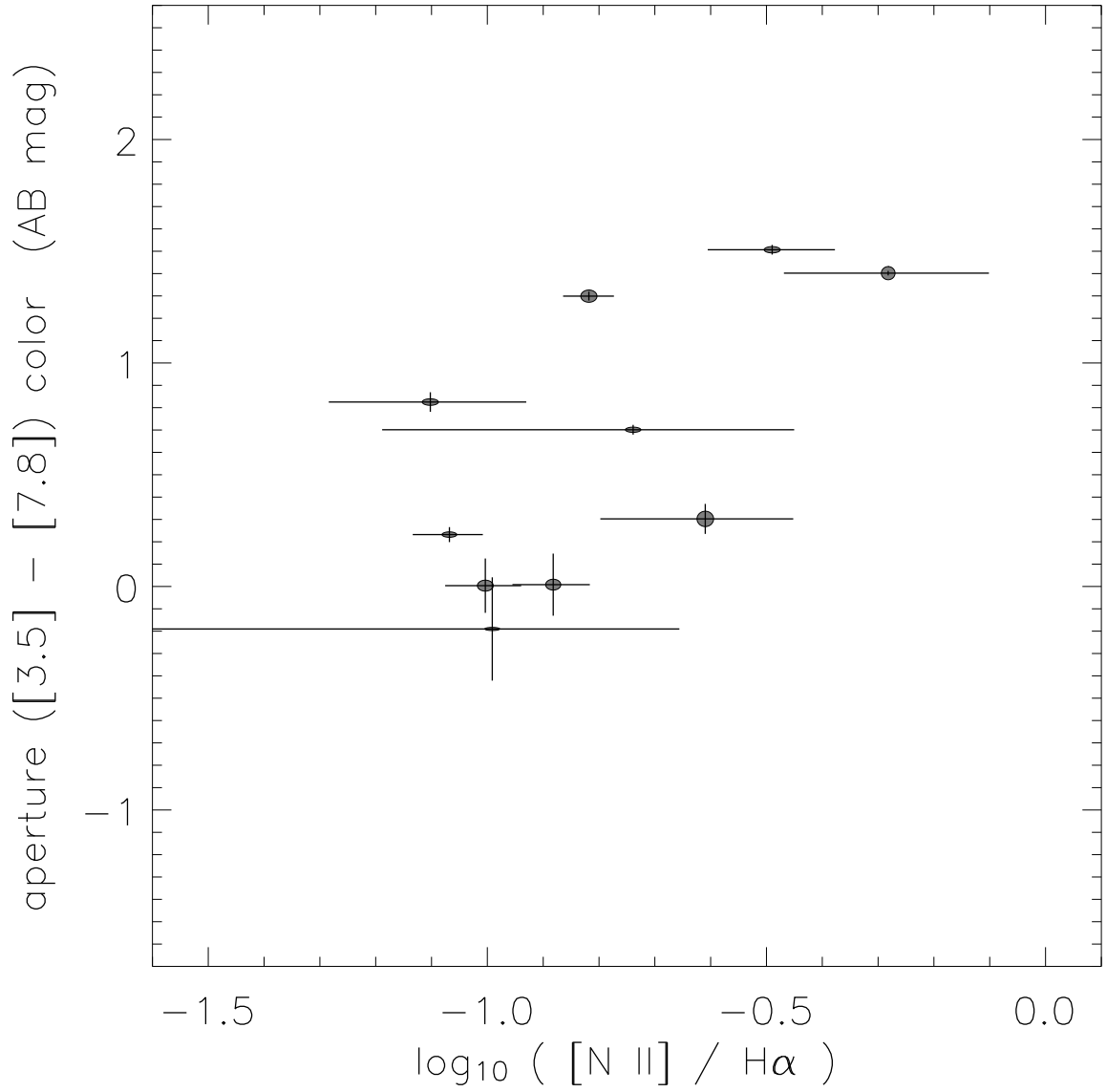


Fig. 4.— Spitzer IRAC observed-frame color as a function of metallicity indicator [N II]/Hα (see text for details) for the low-luminosity galaxies—galaxies with rest-frame visual absolute magnitude $M_{0.1i} > -19.0$—for which the ratio is measured significantly. Symbols as in Figure 1.

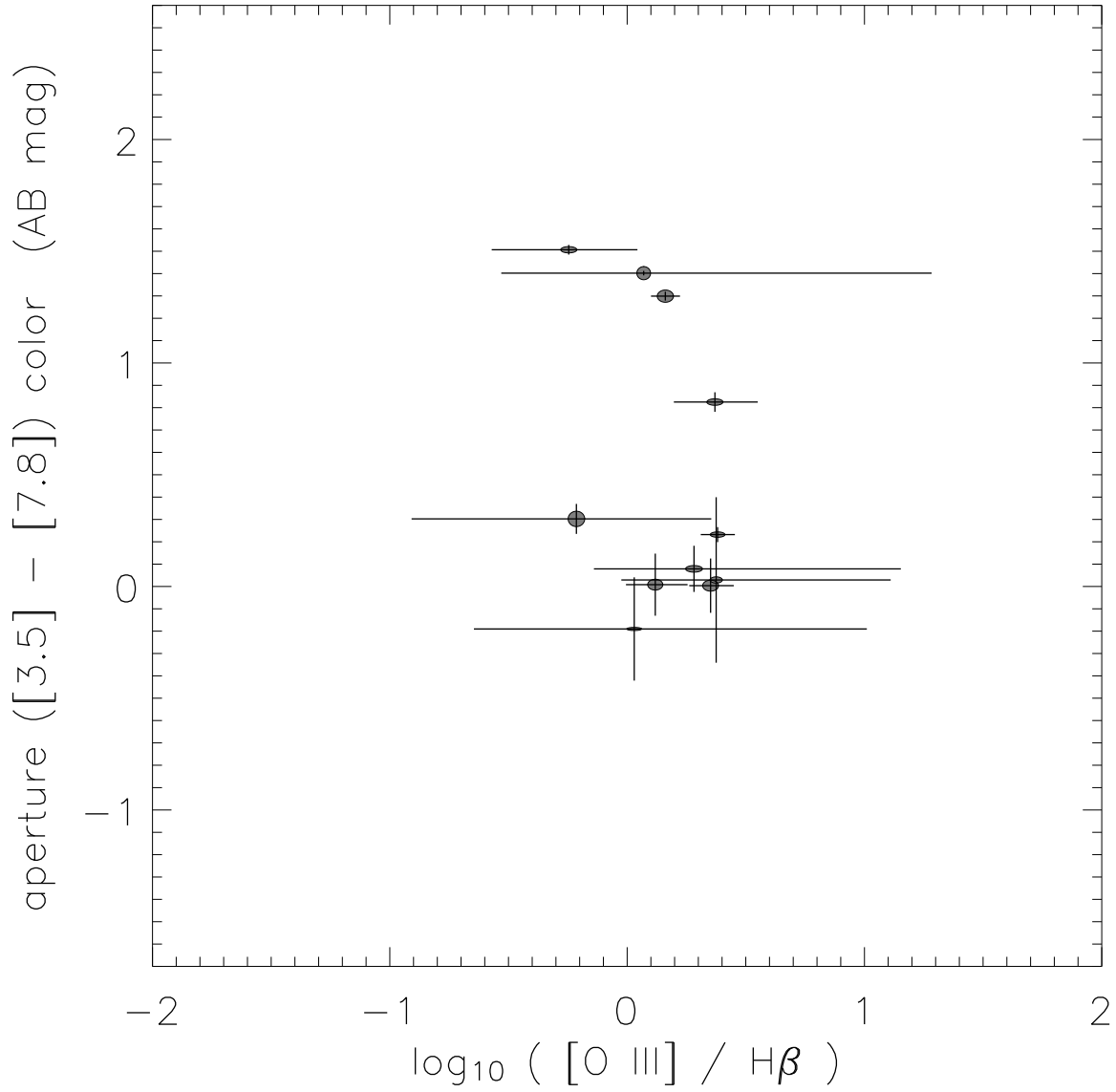


Fig. 5.— Spitzer IRAC observed-frame color as a function of radiation hardness indicator [O III]/Hβ (see text for details) for the low-luminosity galaxies—galaxies with rest-frame visual absolute magnitude $M_{0.1_i} > -19.0$—for which the ratio is measured significantly. Symbols as in Figure 1.

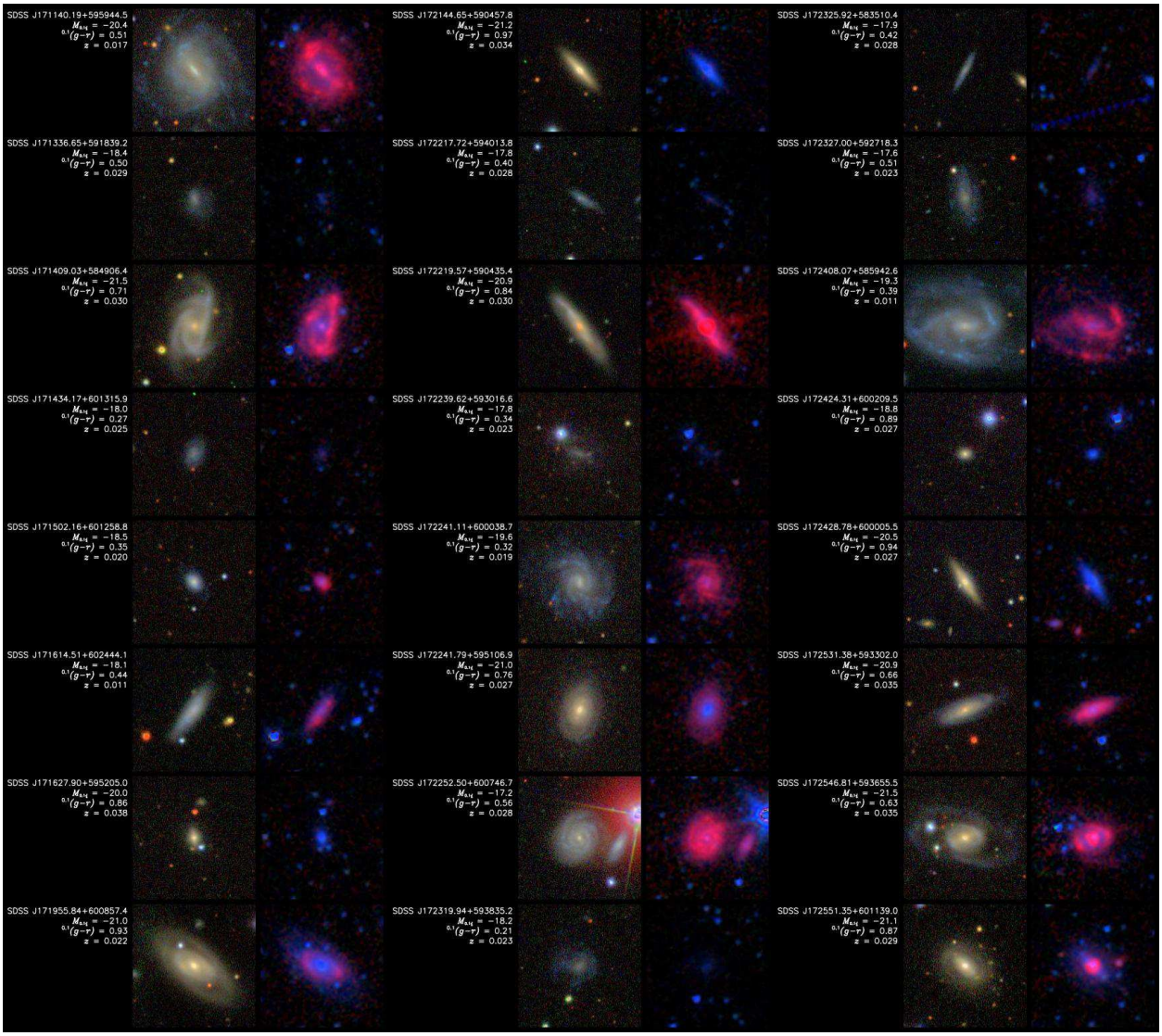


Fig. 6.— Selected low-redshift galaxies from the sample. True-color RGB images made from 73×73 arcsec^2 cutouts of (left) SDSS i, r, and g band mosaics, and (right) Spitzer IRAC [7.8], [4.5], and [3.5] band mosaics from the Spitzer Post-BCD pipeline. The images are made with identical color-preserving stretches (Lupton *et al.* 2004). In the Spitzer IRAC pictures, stellar light appears blue, and interstellar PAH emission appears red.